Published in : Sustainable Energy & Fuels (2020), pp. 1–10
DOI: 10.1039/D0SE00531B
Status : Postprint (Author's version)

Proton Trap Effect on Catechol-Pyridine Redox Polymer Nanoparticles as Organic Electrodes for Lithium Batteries

Antonela Galastegui,[a] Daniela Minudri,[a] Nerea Casado,[b] Nicolas Goujon,[b] Fernando Ruipérez,[b] Nagaraj Patil,[c] Christophe Detrembleur,[d] Rebeca Marcilla,[c] David Mecerreyes [b,*]

[a.] *Instituto de Investigaciones en Tecnologías Energéticas y Materiales Avanzados (IITEMA), Universidad Nacional de Río Cuarto and Consejo Nacional de Investigaciones Científicas y Tecnológicas (CONICET), Campus Universitario, 5800 Río Cuarto, Argentina.*

[b.] *POLYMAT University of the Basque Country UPV/EHU, Av. Tolosa 72, 20018, San Sebastian, Spain.*

[c.] *Electrochemical Processes Unit, IMDEA Energy, Avenida Ramón de la Sagra 3, 28935 Móstoles, Madrid, Spain.*

[d.] *Centre for Education and Research on Macromolecules (CERM), CESAM Research Unit, University of Liege, Allée de la Chimie B6A, 4000 Liège, Belgium.*

Organic redox-active materials are actively being searched as a more sustainable alternative to traditional inorganic cathodes used in rechargeable batteries. Among the different types of organic cathodes, redox polymers based on catechol groups show high energy storage capacities. In this article, we show how the introduction of pyridine groups can shift the potential of catechol containing polymers towards more positive values further enhancing their energy storage capacities. For this purpose, we carried out the synthesis of redox-active polymer nanoparticles having catechol and pyridine functionalities. Spherical nanoparticles between 150 and 300 nm were synthesized by a surfactant-free emulsion polymerization method by copolymerization of dopamine methacrylamide and 4-vinyl pyridine. The chemical composition of the nanoparticles was confirmed by FTIR spectroscopy which shows the presence of a catechol-pyridine hydrogen bonding. Thermal analyses (DSC, TGA) confirmed the glass transition of the nanoparticles between 158 and 190 °C and high thermal stability with a degradation temperature of 300 °C at 5% weight loss ($T_{d5\%}$). The electrochemical characterization of the redox-active polymer nanoparticles show that the redox potential of the catechol group was not affected by the presence of the pyridine in acidic electrolytes ($E_{1/2}$=0.45 V versus Ag/AgCl). However, in organic electrolytes containing a lithium salt the redox potential of the catechol nanoparticles shifted from 0.36 V for catechol homopolymer, to 0.56 V for catechol-pyridine copolymer. This positive potential gain could be associated to the proton trap effect as indicated by DFT calculations. Finally, the beneficial effect of the proton trap effect onto the performance of lithium-ion– polymer battery was demonstrated. The lithium vs. polymer cells showed a promising practical high voltage organic cathode (3.45 V *vs* Li^+/Li), excellent rate performance (up to 120 C) and high capacity retention after cycling (74% after 800 cycles).

Introduction

Organic materials are actively being investigated as an alternative to the metal-oxide based lithium intercalation compounds used in current lithium-ion batteries.[1-4] Inorganic metal oxide cathodes present recycling limitations due to the presence of scarce or toxic metals (Co, V, Ni, etc.). As an alternative, organic redox materials have been proposed due to their potential sustainability and recyclability[5-8] as well as higher theoretical capacity values of up to 600 mA h/g, as compared to inorganic cathodes (typically, <250 mA h/g).[5]

However, in most cases the redox potential of the organic materials is low leading to a low output voltage, and thus low energy density of the battery. Furthermore, in most organic batteries, the cycle stability is poor due to the degradation and/or the dissolution of the organic electrode materials, especially small molecules, in the electrolyte

Published in : Sustainable Energy & Fuels (2020), pp. 1–10
DOI: 10.1039/D0SE00531B
Status : Postprint (Author's version)

during cycling. To mitigate this dissolution issue, redox polymers such as conducting polymers, radical polymers, sulfur polymers or carbonyl polymers which are commonly less soluble, have been investigated.[9] More recently, the use of cross-linked redox polymer nanoparticles (RPNs) was proposed as a way to further avoid the electrode dissolution.[10]

Among the different types of redox polymers, quinone-containing polymers are very popular because of their high theoretical capacity (up to 496 mA h/g) and their high redox potential at around 2.8 V (*p*-benzoquinone) and 3.0 V (*o*-quinones) versus Li/Li^+.[11,12] The redox mechanism of such quinone-containing polymers in organic electrolytes containing Li salts consists of the reversible reduction of quinone to hydroquinone dilithium salt using two electrons and two Li^+ cations. In a seminal work, Detrembleur et al. reported that catechol-containing linear copolymers show a high redox potential of 3.3 V versus Li/Li^+. Furthermore, the electrochemistry was very robust and battery cathodes with a record energy density for polymers up to 1200 W h/kg and high cyclability were demonstrated.[13-18]

On the other hand, Sjödin et al. recently proposed the proton trap concept as a method to increase the stability and the potential of poly(3,4-ethylenedioxythiophene) (PEDOT) conducting polymers containing hydroxyquinone moieties. This method consisted in the inclusion of pyridine groups which interacted with the hydroxyquinone and affected positively the redox process of the hydroxyquinone/quinone redox couple. The presence of pyridine provoked a positive shift in the redox potential and improved the stability of the redox process which allowed to maximize the capacity utilization of the copolymers. The proposed role for the pyridine acceptor was to assist the quinone/hydroquinone redox reaction by accommodating its protons during cycling in aprotic electrolytes.[19]

Due to the chemical similarities between hydroxyquinone (1,4-dihydroxybenzene) and catechol (1,2-hydroxybenzene), we hypothesized that the proton trap effect may take place also in catechol containing polymers. So, the main goal of this article is to investigate the effect of the presence of pyridine groups on the electrochemistry of catechol polymers. Interestingly, since the redox potential of catechol groups takes place at a much higher potential than the conventional quinones, the shift produced by the proton trap effect into catechol polymers should lead to organic materials with very high output voltage (thus, energy density) of the battery. For this purpose, we report here the synthesis and characterization of catechol-pyridine functional redox polymer nanoparticles. Different from our previous article where the synthesis of polycatechol nanoparticles involved tedious protection/deprotection steps, [10] here, the synthesis of the catechol/pyridine nanoparticles was carried out following a much simple one pot/one step process. The so obtained catechol-pyridine redox polymer nanoparticles were fully characterized by physico-chemical and electrochemical techniques. Particular attention was paid to investigate the electrochemical behaviour of the catechol polymer in different electrolytes to elucidate the effect of pyridine group in the redox process and to confirm or deny the proton trap effect. To end up, the catechol-pyridine RPNs were investigated as cathode materials for lithium metal batteries.

Experimental

Materials

4-Vinyl pyridine (VP) 2,2´-azobis(2-methylpropionamidine) dihydrochloride (AIBA), 1,2-dimethoxyethane (DME; 99.5%, Sigma Aldrich), 1,3-dioxolane (DOL; 99.8%, Sigma Aldrich), thin multi-walled carbon nanotubes (CNTs; Elicarb® MW, Thomas Swan), polyvinylidene fluoride (PVDF) and N-methylpyrrolidone (NMP) were purchased from Sigma Aldrich. Dopamine-HCl and $MgSO_4$ were obtained from Alfa Aesar. $AgNO_3$, $LiClO_4$, methanol, ethyl acetate, acetonitrile (MeCN) and absolute ethanol were purchased from Acros. LiTFSI was obtained from Solvionic. Carbon

Published in : Sustainable Energy & Fuels (2020), pp. 1–10
DOI: 10.1039/D0SE00531B
Status : Postprint (Author's version)

paper (Toray TP-060, QUINTECH) and lithium foil were purchased from PI-KEM and Sigma Aldrich, respectively. Carbon black C65 (Super C65) was obtained from Timical. All the chemicals and solvents were employed as received without further purification.

Dopamine methacrylamide (DMA) was synthesized by a protocol described by Nguyen et al.[20] The monomer was successfully characterized by proton NMR analysis. ^{1}H-NMR (DMSO-d_6, 400 MHz): δ 8.7–8.6 (2H), 7.9 (1H), 6.4–6.6 (2H), 6.42 (1H), 5.62 (1H), 5.31 (1H), 3.24 (2H), 2.51 (2H), 1.85 (3H) (Figure S1).

Synthesis of catechol-pyridine RPNs

RPNs were synthesized by surfactant-free emulsion polymerization (SFEP) in aqueous media at 70 ºC, employing unprotected DMA through a modified procedure proposed by Xue et al.[21], a work that employed DMA at 1 wt. % only as a cross-linker of the polymeric chains, while the synthesis of poly(DMA) could not be properly achieved.

In the synthesis we propose, Scheme 1, a certain amount of VP (depending on the ratio with the catechol monomer) and 0.03 mmol (1x10^{-3} M) of AIBA pre-dissolved in 25 mL of Milli Q water were mixed under vigorous stirring with a deoxygenation process employing N_2 during 30 min. At 55 ºC, a solution of unprotected DMA dissolved in methanol (0.1 g/mL,) was injected at 2 mL/min into the reaction mixture employing an automatic syringe pump, the amount of milliliters incorporated will depend on the molar fraction ratio between DMA and VP. At the end of the injection, the reaction mixture reached 70 ºC, which was left during 6 h. A total monomer concentration of 1 mmol (4x10^{-2} M) was employed. The nanoparticles were then purified with Milli Q water during 3 days at 25 ºC employing dialysis tubes with a molecular weight cutoff of 14000 Da and finally freeze-dried with a Telstar LyoQest-85 Lyophilizer at -80 ºC and 0.089 mbar during 3 days.

Characterization techniques

The hydrodynamic diameter of the catechol-pyridine RPNs were measured by dynamic light scattering (DLS) using a Malvern Zetasizer Nano ZS. A drop of reaction mixture (~0.1 mL of the dispersion in water) was diluted with 1 mL of Milli Q water employing disposable polystyrene cuvettes DTS0012. The intensity average was measured at 25 ºC and 173 ° backscatter angle by using dynamic light scattering Malvern ZetaSizer Nano-S instrument equipped with a 633 nm red laser.

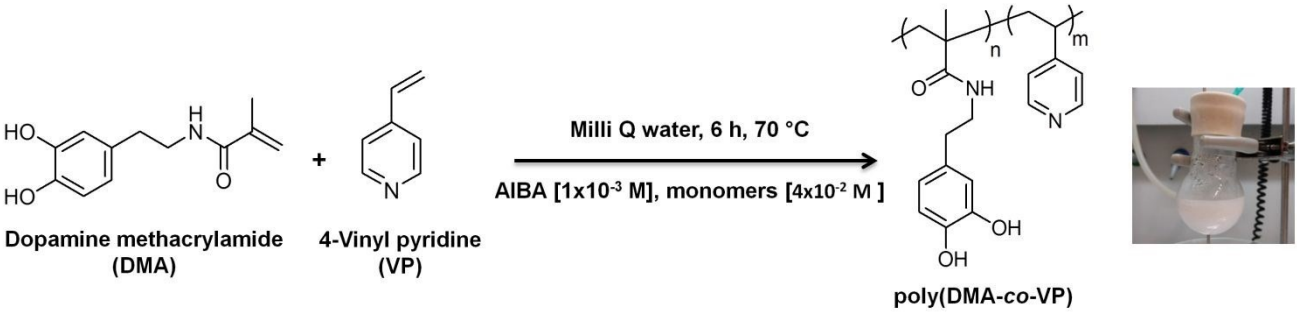

Scheme 1. Synthesis of the RPNs by SFEP in aqueous solution.

The diameter and the morphology of the dried nanoparticles were measured by transmission electron microscopy (TEM) employing a TECNAI G2 20 TWIN (200 kV). The samples were deposited on copper grids and left dry at room temperature. Fourier transform infrared (FTIR) spectra were measured on a Bruker Alpha II spectrophotometer employing Platinum ATR module with diamond window.

The thermal stability of the RPNs was investigated by thermogravimetric analysis (TGA) performed on a TGA Q500 from TA Instruments. The samples were heated at 10 ºC/min under N_2 atmosphere from room temperature to 800

Published in : Sustainable Energy & Fuels (2020), pp. 1–10
DOI: 10.1039/D0SE00531B
Status : Postprint (Author's version)

ºC. Differential scanning calorimetry (DSC) was employed to detect the Tg of the samples by measurements on a DSC Q2000 from TA Instruments. The DSC scans were performed at heating and cooling rates of 10 ºC/min from -25 ºC to 200 ºC.

Electrochemistry in 3-electrode cells

10 mg of redox-active catechol-pyridine polymer nanoparticles (60 wt. %), 5 mg of conductive carbon black C65 (30 wt. %) and 1.8 mg of PVDF (10 wt. %) were dispersed in 400 µL of NMP by magnetic stirring for 15 min to form a uniform suspension. The slurry (3 µL) was dropped on the top of the glassy carbon electrode (GC) and dried in vacuum at 50 °C for 1 h. The electrode was used immediately after drying as working electrode. Before modification, the GC electrode was polished using 0.3 µm alumina and sequentially sonicated in water and absolute ethanol.

Cyclic voltammetry (CV) measurements were performed in three different electrolytes using an Autolab PGSTAT204 potentiostat/galvanostat, in a three-electrode configuration. The working electrode was the modified glassy carbon disk, a platinum wire was used as a counter electrode (CE) and Ag/AgCl (3 M KCl) was used as a reference electrode in aqueous medium (0.1 M $HClO_4$ and 0.1 M LiTFSI), whereas that in organic medium (0.1 M $LiClO_4$/MeCN) the reference electrode was Ag/Ag^+ ($1x10^{-2}$ M $AgNO_3$ in MeCN). Before each measurement, the electrolyte solutions were bubble for 5 minutes with N_2.

Preparation of catechol-pyridine polymer nanoparticles/CNTs cathode for Li-ion half-cells

5 mg of CNTs were dispersed in 3 mL NMP using a tip sonicator, followed by addition of 11.5 mg of polymer nanoparticles, proceeding to sonication for 2 h in a bath sonicator (Branson 2510, 100 W, 42 kHz) and overnight stirring to prepare the electrode slurry. This viscous smooth slurry was then coated onto carbon paper current collector by drop-casting, dried overnight at 50 °C under vacuum and cut into 12-mm disks. Typically, the polymer loading on carbon paper electrode was found to be 1.8–1.9 mg cm^{-2} (~70 wt% CNTs).

Electrochemical characterization of catechol-pyridine RPNs as cathodes in Li-ion half cells

The obtained cathodes were tested in a Li-ion half cell configuration assembled into CR 2032 coin-type cells using a lithium foil anode and a pair of porous Whatman glass microfiber filters (Grade GF/B) soaked with ~200 µL of electrolyte (1 M LiTFSI in dried and degassed DME/DOL (1:1 v/v)). The cells were assembled in a high-purity argon-filled glovebox (MBraun; H_2O < 0.5 ppm and O_2 < 1.5 ppm) to avoid any possible contamination by oxygen and moisture. The CV of Li-ion half-cells was performed with a Bio-logic

VMP3 multichannel Potentiostat/Galvanostat (Biologic SP150). The cycling and rate performance of coin-type Li-ion halfcells were assessed by galvanostatic charge–discharge (GCD) experiments with a Neware battery cycler at 25 °C. As a commonly used procedure for polymer-based organic batteries, the specific capacities and current rates (C-rates) were normalized with respect to the mass of polymer in the cathode.

Quantum chemical calculations

All geometry optimizations were performed in gas phase within density functional theory (DFT) using the B3PW91 functional;[22-24] together with the 6-31+G(d,p) basis set.[25] Harmonic vibrational frequencies were obtained to confirm that all structures were minima (no imaginary frequencies) in the potential energy surface. The frequencies were then used to evaluate the zero-point vibrational energy (ZPVE) and the thermal (T = 298 K) vibrational corrections to the enthalpy and Gibbs free energy in the harmonic oscillator approximation. Single point calculations using the aug-cc-pVTZ basis set were carried out on the optimized structures to refine the electronic

Published in : Sustainable Energy & Fuels (2020), pp. 1–10
DOI: 10.1039/D0SE00531B
Status : Postprint (Author's version)

energy.[26] Solvent effects in acetonitrile have been estimated using the polarizable continuum model (PCM) approach.[27-30] All calculations were performed using the Gaussian 16 suite of programs.[31]

Results and discussion

Synthesis and characterization of redox-active catechol-pyridine polymer nanoparticles (RPNs)

Redox-active catechol-pyridine polymer nanoparticles (RPNs) were synthesized by emulsion polymerization, as described in Scheme 1. The synthesis was carried out by a surfactant-free emulsion polymerization recently reported for the synthesis of catechol functional microgels.[21] It is well known that the catechol groups traps the growing radical during free-radical polymerization. However, this fact did not limit the reaction conversion and it was observed that cross-linked micro-nano particles were obtained due to the coupling between catechol radicals. In a typical reaction, the two monomers dopamine methacrylamide (DMA) and 4-vinyl pyridine (VP) were copolymerized simultaneously in water using AIBA as radical initiator leading to almost quantitative yields after 6 h at 70 ºC. Using this synthetic route, three different catechol-pyridine polymer nanoparticles were synthesized with different monomer molar compositions: poly(DMA_{66}-*co*-VP_{33}), poly(DMA_{50}-*co*-VP_{50}) and poly(DMA_{33}-*co*-VP_{66}) (the subscripts represent the composition of each monomers). Poly(catechol methacrylamide) homopolymer named poly(DMA) was also synthesized following the same route. It is important to remark that this method led to the one-pot synthesis of catechol polymer nanoparticles in one step process, without the need of additional protection/deprotection steps. Worth mentioning that DMA, besides of being a biomimetic monomer, also acts as a cross-linker since it is known that the radical polymerization of unprotected catechol-bearing vinyl monomers is expected to provide (hyper)branched polymers, or even more, cross-linked materials.[32] Therefore, in a onestep reaction and in aqueous medium, the nanoparticles were synthesized with the advantage of not needing the employment of a surfactant and an additional cross-linker.

Table 1. Redox-active catechol-pyridine nanoparticles (RPNs)

Nanoparticle	Yield[1] (%)	Size[2] (nm)	PDI	Size[3] (nm)	Tg[4] (°C)
Poly(DMA)	93	166.8	0.011	156.7	158
poly(DMA_{66}-*co*-VP_{33})	90	188.9	0.038	147.6	184
poly(DMA_{50}-*co*-VP_{50})	92	291.3	0.061	257.9	182
poly(DMA_{33}-*co*-VP_{66})	89	309.6	0.052	304	187

[1] Yield obtained by gravimetry, [2] Hydrodynamic diameter determined by DLS in water, [3] Size of the dried RPN as measured by TEM, [4] Glass transition temperature (Tg) as measured by DSC in the second scan at a rate of 10 ºC/min.

The hydrodynamic diameter of the NPs within the aqueous latex was determined by Dynamic Light Scattering (DLS) and their dried size by Transmission Electron Microscopy (TEM). In all the cases the particles showed sizes between 150 and 300 nm. Both techniques are compared in Table 1. As the vinyl pyridine content increases in the composition of the NPs, the hydrodynamic diameter obtained by DLS and the size observed in TEM images also

Published in : Sustainable Energy & Fuels (2020), pp. 1–10
DOI: 10.1039/D0SE00531B
Status : Postprint (Author's version)

increases. The polydispersity index (PDI) obtained by DLS was low for all the nanoparticles. As expected, the NP size detected by TEM was slightly lower than in the case of DLS technique, since TEM represents dried nanoparticles, indicating that the nanoparticles were in a swollen state in aqueous solution. The catechol-pyridine polymer nanoparticles showed a spherical shape, as it can be seen in the TEM images (Figure 1). Relatively monodispersed dried nanoparticles were obtained with particle size ranging from 150 to 300 nm with increasing sizes at higher vinyl pyridine content.

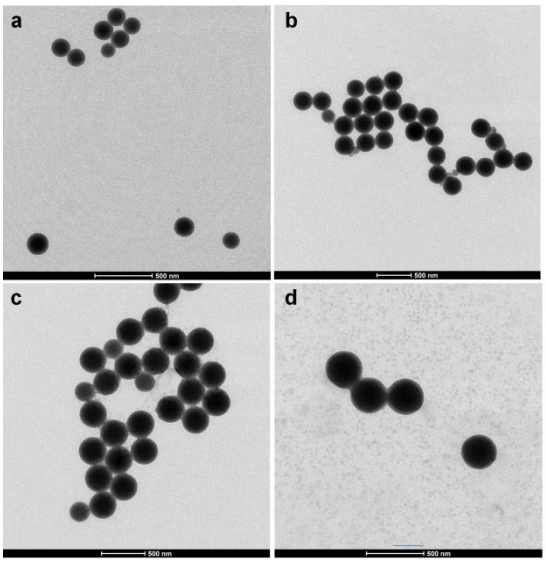

Figure 1. TEM images of poly(DMA) (a), poly(DMA_{66}-*co*-VP_{33}) (b), poly(DMA_{50}-*co*-VP_{50}) (c) and poly(DMA_{33}-*co*-VP_{66}) (d). Scale bar: 500 nm.

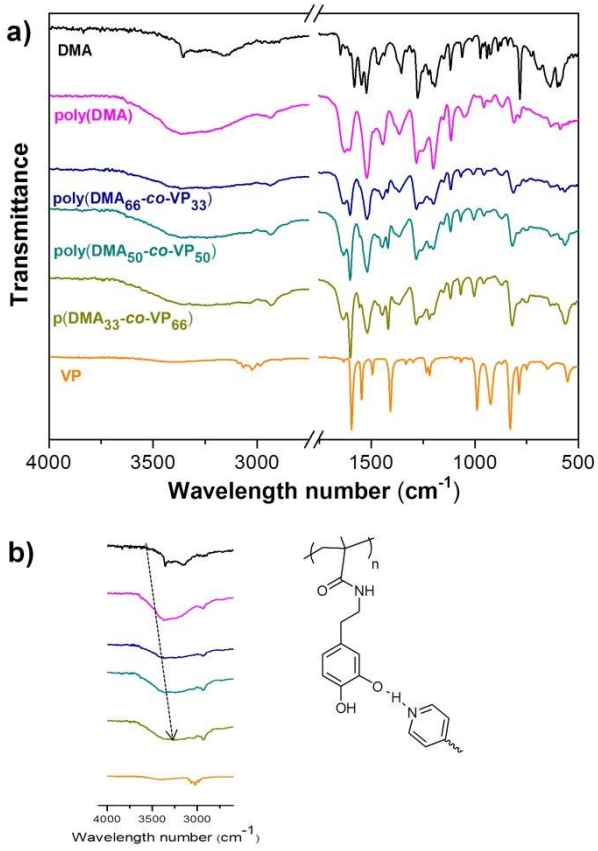

Figure 2. (a) FTIR spectra of the initial monomers dopamine methacrylamide (DMA) and 4-vinyl pyridine (VP) and the synthesized RPNs hydrogen bond interaction between catechol and pyridine groups (b) Amplification of the range between 4000 and 3000 cm^{-1}

Published in : Sustainable Energy & Fuels (2020), pp. 1–10
DOI: 10.1039/D0SE00531B
Status : Postprint (Author's version)

FT-Infrared Spectroscopy (FTIR) was carried out to corroborate the chemical composition of the RPNs. The spectra are provided in Figure 2a. The band at 785 cm^{-1} from DMA belongs to the bending vibration of the vinyl group (s; ν_s (C=C vinyl), which disappears after polymerization. The bands at 923 and 783 cm^{-1} belong to vinyl bend vibrations of VP, which also disappear after the RPNs synthesis, confirming the radical polymerization. A strong broad peak is observed in all RPNs at 1638 cm^{-1} due to the amide carbonyl group stretching vibration (s; ν_s (HN-C=O)), this peak can be observed at 1645 cm^{-1} in DMA monomer. Characteristics bands of DMA are present in all the nanoparticles: the peaks at 1522 and 1277 cm^{-1} are characteristics from the catechol moiety (m; ν_s (C=C arom.)).[33,34] Some characteristic vibrations of the pyridine ring are present in all the copolymers: peaks at 1600, 1545 and 1410 cm^{-1} from the aromatic structure.[35] The hydrogen bonding interaction between DMA and VP is clearly observed in the range between 4000 and 3000 cm^{-1}: the spectrum of poly(DMA) exhibits a broad peak mainly originated from the hydroxyl groups of the catechol. While in the copolymers it is noticed that the center of this region shifts from 3365 to 3165 cm^{-1}, a lower wave number region compared to the homopolymer, observed in the Figure 2b (an amplification of the region). The shift indicates that the inter-associated

View Article Online

hydrogen bonds between VP and DMA are stronger than the DOI: 10.1039/D0SE00531B self-associated hydrogen bonds in the pure polymers, as explained by Salim et al.[36] and Kuo et al.[37] Also, the band at 990 cm^{-1} can be used to identify the presence of hydrogen bonding interactions between the hydroxyl groups of DMA and the pyridine group; this band corresponds to the aryl CH bending of the pure pyridine ring, which shifts to 1004 cm^{-1} in the presence of DMA. Both peaks, or regions, indicate the formation of hydrogen bond between DMA and VP in the nanoparticles as expected from the well known interaction between pyridine and phenol groups.[37] All in all, the chemical composition of the RPNs as well as the strong catecholpyridine interaction by hydrogen bonding is confirmed by FTIR. The thermal behavior of the catechol-pyridine RPNs was analyzed by Thermogravimetric Analysis (TGA) and Differential Scanning Calorimetry (DSC) shown in Figure S2-3. From the TGA results, it can be appreciated that the RPNs almost quantitatively degrade at temperatures between 350 and 420 ºC with a degradation temperature of 300 ºC at 5 % weight loss ($T_{d5\%}$). The degradation temperature increases with the VP presence**.** Furthermore, a weight loss between 3 and 10 wt% is observed at low temperature which could be due to the hygroscopic nature of the NPs and the adsorbed water. Furthermore, the NPs show a residue at 700 ºC between 10 and 20 % which is higher at increased DMA composition.

DSC was measured for all the RPNs (Figure S3). The copolymers presented a higher glass transition temperature (Tg) than the homopolymer: poly(DMA_{66}-*co*-VP_{33}), poly(DMA_{50}*co*-VP_{50}) and poly(DMA_{33}-*co*-VP_{66}) showed a difference of ~30 ºC with poly(DMA), which showed a Tg of 158 °C. The hydrogen bond interaction generated and the presence of VP may play a key role in the mobility of the chains, increasing Tg values.[37,38] It was interesting to notice that the observed Tg value in this work, for poly(DMA), is similar to a Tg of ~160 °C value reported by Yang et al., as obtained by free radical polymerization employing unprotected DMA in DMF.[39]

Electrochemical characterization of redox-active catechol-pyridine polymer nanoparticles

The fundamental electrochemical behaviour of all redox-active catechol-pyridine polymer nanoparticles (RPNs) was assessed in aqueous electrolytes (0.1 M $HClO_4$ and LiTFSI in water) as well as in organic media (0.1 M LiTFSI in MeCN). The goal was to investigate how the RPNs respond to different electrolyte environments and the effect that the catechol and pyridine composition produce on the redox behaviour of the nanoparticles. Cyclic voltagrams (CV) were recorded at 20 mV/s scan rate in the acidic electrolyte medium (Figure 3a), all nanoparticles showed a reversible peak corresponding to the reversible catechol redox reaction (Figure 3b). Poly(DMA) showed a half-wave potential ($E_{1/2}$) of 0.45 V versus Ag/AgCl, and when the pyridine content in RPNs increased, a small decrease of $E_{1/2}$

Published in : Sustainable Energy & Fuels (2020), pp. 1–10
DOI: 10.1039/D0SE00531B
Status : Postprint (Author's version)

(for instance, $E_{1/2}$=0.43 V for poly(DMA_{33}-*co*VP_{66})) was observed. The similar reduction potential and oxidation potential in all the cases suggests that redox reactions are facile in the homopolymer and all the copolymers.

To know if the reaction is controlled by diffusion or surface processes, we carried out a study of the peak current as a function of the scan rate. I_p was plotted versus scan rate and then as a function of the square root of the scan rate (Figure S4-5 respectively). No linear correlation was observed in the first case, so the reaction is not controlled by surface processes. However, in the second case, it is possible to observe a linear dependence of both parameters; this is a typical diffusion controlled reaction. Besides, from the slope of the lines it is possible to derive that the cathodic diffusion coefficient and anodic diffusion coefficient of poly(DMA) are higher than the values for all copolymers. The well-maintained contact between the redox-active nanoparticles and the electrolyte allows rapid ion diffusion, and rapid load transfer kinetics through the electrode.

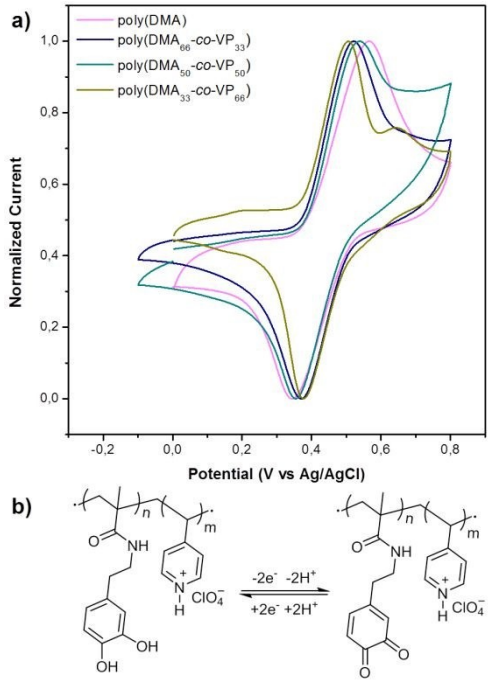

Figure 3. a) Cyclic voltammetry of redox-active catechol-pyridine nanoparticles at 20 mV/s in acidic aqueous electrolyte (0.1 M $HClO_4$), (b) Schematic representation of reversible redox reaction mechanism of catechol-pyridine nanoparticles in acidic electrolytes.

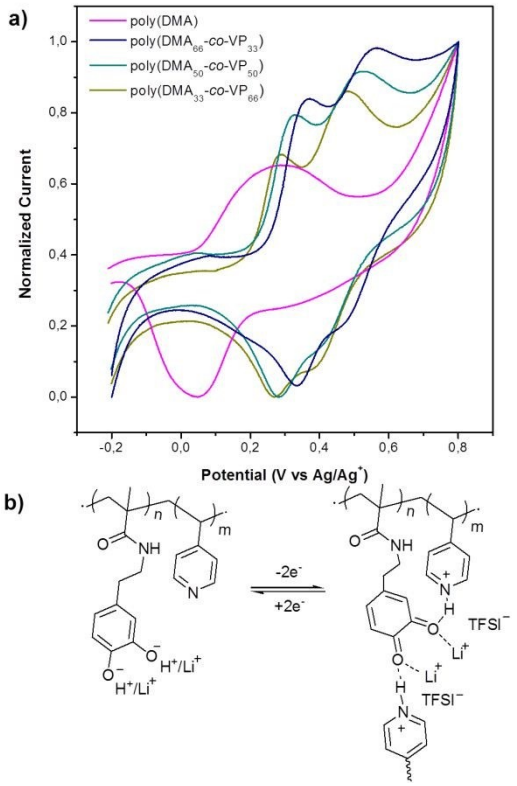

Figure 4. Cyclic voltammetry of redox-active catechol-pyridine nanoparticles at 20 mV/s in (a) organic electrolyte (0.1 M LiTFSI – MeCN) (b) Schematic representation of redox process along with the proton trap mechanism.

It is confirmed that the quinone redox chemistry presents a definite and reversible peak in protic electrolyte with a two-electron transfer process and the potential redox is not significantly affected by the presence of the pyridine group which in acidic media it is in its protonated state.[13] While the copolymers have larger nanoparticles size and electrostatic interaction of pyridine with acidic media that decreases the charge transfer process.

Interestingly, the cyclic voltammetry of RPNs in aqueous electrolyte containing a lithium salt as well as in organic electrolyte containing a lithium salt presented a different behaviour. Figure 4a (organic electrolyte) and Figure S6 (aqueous electrolyte) and report the normalized peak currents recorded at a scan rate of 20 mv s^{-1}. Whereas the poly(DMA) homopolymer showed only one oxidation/reduction peak, it is possible to see two oxidation peaks shifted to higher potential for all copolymers. A closer look into the cyclic voltammetry of the RPNs in acetonitrile containing LiTFSI (Figure 4a) showed a single oxidation peak at 0.27 V vs Ag/Ag^+ (0.01 M $AgNO_3$ in CH_3CN) for poly(DMA), whereas poly(DMA_{66}-*co*-VP_{33}) was characterized by two peaks with a clear displacement to a higher potential. The corresponding peak potentials were at 0.36 V and 0.56 V vs Ag/Ag^+. However, when the amount of

Published in : Sustainable Energy & Fuels (2020), pp. 1–10
DOI: 10.1039/D0SE00531B
Status : Postprint (Author's version)

pyridine increases, the oxidation peak potentials exhibit a slight decline, so poly(DMA_{33}-*co*-VP_{66}) presents the two peaks at 0.3 V and 0.48 V vs Ag/Ag^+.

A similar behavior was observed in aqueous neutral electrolytes (Figure S6) where the poly(DMA) shows only a peak at 0.34 V vs Ag/AgCl whereas the copolymers showed two peaks at more positive potentials. In both cases the appearance of two oxidation/reduction peaks may be due to the different stability of intermediates generated in the reaction for the loss of each of the catechol's protons, and the corresponding pyridine proton trap effect (Figure 4).[40]

In order to further corroborate the mentioned pyridine proton trap effect, density functional theory (DFT) calculations were performed using a simplified model of the copolymer. The simulations show a hydrogen-bonding interaction between the hydrogens of the catechol (QH_2) and the pyridines, as well as between the carbonyls of the oxidized quinone (Q) and the protonated pyridine, as it can be observed from the geometrical parameters in Table 2 and Figure S7. Thus, in the reduced state, $N_{py}\cdots HO$ bond distances of 1.850 and 1.806 Å are calculated, within range of hydrogen bonding. In the oxidized state, the protons of the catechol are transferred to the pyridines, and the calculated NH···O=C bond distances are 1.797 and 1.775 Å. This means that the hydrogen bonding interactions are stronger in the oxidized state.

Table 2. Geometrical parameters of the model copolymer during a redox cycle. Bond distances (R_e) in Å.

	$R_e(N_1H_1)$	$R_e(O_1H_1)$	$R_e(N_2H_2)$	$R_e(O_2H_2)$
QH_2[a]	1.850	0.990	1.806	0.991
SQ[b]	1.091	1.492	1.589	1.036
Q[c]	1.036	1.797	1.037	1.775

[a]Catechol. [b]Semiquinone. [c]Quinone

Besides, the proton trap effect imparts a positive consequence to shift the redox potentials to higher values. The redox potential obtained by DFT calculations is increased from 0.02 V (vs SHE) in the bare catechol to 0.77 V in the copolymer with pyridines. As expected this values are far from the experimental conditions due to the theoretical calculation parameters. However, the potential shift is clearly observed. A possible explanation is that the hydrogen bonding may promote the donation of the catechol protons to the pyridine and, thus, facilitating the oxidation to the quinone state, which is further stabilized by the new hydrogen bonds established with the protonated pyridines.

Redox-active catechol-pyridine polymer nanoparticles as cathodes in lithium batteries

The ability of pyridine groups to increase the redox potential of catechol containing nanoparticles in aprotic electrolytes is expected to be beneficial to implement these materials as high voltage cathodes in electrochemical energy storage systems. For this purpose, we constructed Lithium half-cells by taking poly(DMA_{50}-*co*-VP_{50}) as a representative example from the catechol-pyridine polymer nanoparticles family and compared its electrochemical behaviour with poly(DMA) homopolymer cathode. CVs of both the poly(DMA) and poly(DMA_{50}-*co*-VP_{50}) featured reversible redox behavior with a pair of broad redox peaks centered at $E_{1/2} \approx 3.3$ V (*vs* Li/Li^+) and $E_{1/2} \approx 3.45$ V, respectively (Figure 5a). Interestingly, a relative redox potential gain of ~150 mV in the case of poly(DMA_{50}-*co*-VP_{50}) compared to poly(DMA) is also apparent from these CVs confirming the proton trap effect. This electrochemical behavior is once again in good agreement with the results obtained in three-electrode CV studies with the aqueous neutral and organic electrolyte media containing LiTFSI (Figure 4), further attesting the proton-trap effect at the cell level.

Published in : Sustainable Energy & Fuels (2020), pp. 1–10
DOI: 10.1039/D0SE00531B
Status : Postprint (Author's version)

Interestingly, this redox potential gain imparted by the protontrap comonomers in poly(DMA$_{50}$-*co*-VP$_{50}$) offers a promising practical high voltage organic cathode (3.45 V *vs* Li$^+$/Li), whose value is higher than that of the most of the state-of-the-art poly(catechol)s reported in the literature such as poly(dopamine acrylamide) (1),[13] poly(4-vinyl catechol) (2),[13] polydopamine/FWNTs (4),[14] polydopamine/RGO (5),[15] poly(dopamine-*co*-pyrrole) (6),[16] catechol-derived polyallylamine,[17] and close to that of catechol functionalized poly(vinylimidazolium) polymer (3.47 V, #3 in Figure 5b). [18]

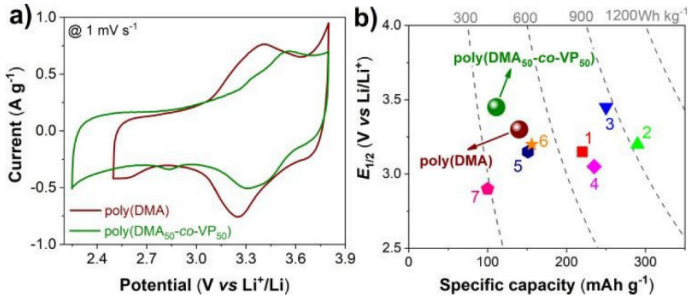

Figure 5. CV profiles (a), and comparison of $E_{1/2}$ of poly(DMA) and poly(DMA$_{50}$-*co*-VP$_{50}$) with the state-of-the-art poly(catechol) cathodes in Li-ion half-cells (b).

The performance of poly(DMA) and poly(DMA$_{50}$-*co*-VP$_{50}$) as organic cathodes was further evaluated by galvanostatic charge–discharge (GCD) experiments in Li-ion half-cell configuration. Figures 6a and b show their comparative rate performance at progressively increasing C-rates of 0.5 C to 120 C. The representative specific capacity–potential profiles are also given in Figure S8. At a low C-rate of 0.5 C, poly(DMA) delivered a reversible discharge capacity of 140 mAh g^{-1} with an initial Coulombic efficiency of 87% and active-material utilization of 58% (theoretical specific capacity of 240 mAh g^{-1}). Interestingly, poly(DMA$_{50}$-*co*-VP$_{50}$) demonstrated both enhanced Coulombic efficiencies (above 92%) and higher active-material utilization of 70% (theoretical specific capacity of 157 mAh g^{-1}), despite a lower discharge capacity of 110 mAh g^{-1}. Due to the rectangular and sloping nature of CV and GCD profiles, respectively, we tentatively evaluated the capacity contribution from the CNT additives. A small capacity contribution of ~15 mAh g^{-1} was noted for this blank electrode, suggesting that majority of the capacity of the composite electrode comes from the redox reactions rather than CNTs (Figure S9).

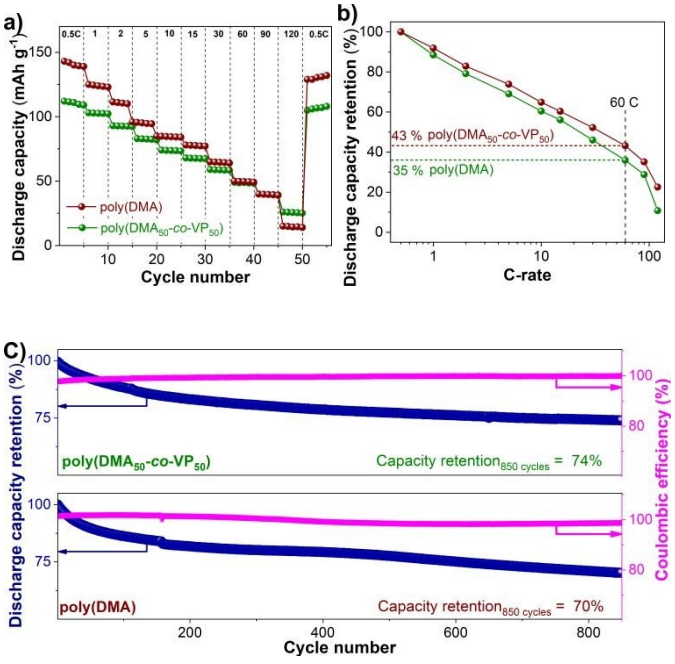

Figure 6. The electrochemical performance of poly(DMA) and poly(DMA$_{50}$-*co*-VP$_{50}$) in Li-ion half-cells. (a, b) Rate performance: discharge capacity vs cycle number (a), discharge capacity retention at different C-rates (b). The discharge capacities at higher C-rates are normalized with respect to the discharge capacity at 0.5 C. (c) Cycle performance: discharge capacities and Coulombic efficiencies measured at 1 C.

With increasing C-rates, both the capacities (Figure 6a) and their capacity retentions (Figure 6b) decreased for both the electrodes, but more drastically in the case of poly(DMA). For instance, at 60 C, poly(DMA) retained 35% of its initial capacity, while poly(DMA_{50}-*co*-VP_{50}) demonstrated higher retention rate of 43%. This is in good agreement with the enhanced redox kinetics anticipated by CV experiments in 3 electrode cells (Figure 4a), where the CV of poly(DMA_{50}-*co*VP_{50}) was characterized by a smaller peak-to-peak voltage separation (~0.05 and ~0.08 V for the 1st and 2nd redox peaks, respectively) than that of poly(DMA) (~0.22 V), thus facilitated kinetics in the case of copolymer. Even at 120 C, poly(DMA_{50}*co*-VP_{50}) delivered higher capacity of 26 mAh g^{-1} compared to the poly(DMA) (15 mAh g^{-1}). Additionally, when the C-rate was brought back to 0.5 C, nearly quantitative capacity recovery was observed in both the cases.

Finally, the cycling stability of of poly(DMA) and poly(DMA_{50}-*co*-VP_{50}) was assessed by GCD studies at 1 C. Both the systems attained stable capacities quickly, and impressively retained 70 and 74% of their initial capacities over a period of 29 days that comprised 850 repeated full charge/discharge cycles (Figure 6c and Figure S10). It is also worth to mention here that after initial few activation cycles, the average Coulombic efficiencies in these cycling tests remained stable at 99±1.

Conclusions

In conclusion, we have demonstrated that the introduction of pyridine groups can shift the redox potentials of catechol containing polymers towards high voltage cathodes in organic electrolytes. This positive potential shift previously observed in [DOI: 10.1039/D0SE00531B] hydroxyquinone functional conducting polymers and named as proton trap effect was corroborated here for catechol functional polymer nanoparticles. We also demonstrated the successful synthesis of spherical nanoparticles by a surfactant-free emulsion polymerization method by copolymerization of dopamine methacrylamide and 4-vinyl pyridine in one step/pot process without the need of protection/deprotection of the catechol groups. The electrochemical characterizations of the redox-active polymer nanoparticles show that the redox potentials of the catechol group were not affected by the presence of the pyridine in acidic electrolytes ($E_{1/2}$=0.45 V versus Ag/AgCl). However, in neutral aqueous/organic electrolytes in the presence of a lithium salt the redox potential of the catechol nanoparticles shifted from 0.36 V (catechol only) to 0.56 V catechol in the presence of pyridine. This shifting of redox potential could be associated to the proton trap effect as indicated by DFT calculations. Finally, the benefit of the proton trap effect on the electrochemical performance of RPNs as cathodes in LIBs was demonstrated. The redox polymer nanoparticles having catechol-pyridine groups showed a promising practical high voltage organic cathode (3.45 V vs Li^+/Li), excellent rate performance (up to 120 C) and superior capacity retention after cycling (74% after 800 cycles).

Acknowledgements

The authors thank for technical and human support provided by IZO-SGI SGIker of UPV/EHU. The authors would like to thank the European Commission for financial support through funding from the European Union's Horizon 2020 research and innovation program under the Marie Sklodowska-Curie grant agreement No 823989. C.D. is FNRS Research Director and thanks the National Funds for Scientific Research (FNRS, Belgium) and CESAM Research Unit (ULiege, Belgium) for funding. R.M. thanks the Spanish Ministry of Science, Innovation and Universities through the SUSBAT project (Ref. RTI2018-101049-B-I00) (MINECO/FEDER, UE) for financial supports. N.P. appreciates Spanish MINECO for the Juan de la Cierva-formation fellowship [FJC2018-037781-I].

Notes and references

1 S. Muench, A. Wild, C. Friebe, B. Haupler, T. Janoschka and U. S. Schubert, *Chem. Rev.*, 2016, **116**, 9438.

2 J. Winsberg, T. Hagemann, T. Janoschka, M. D. Hager and U. S. Schubert, *Angew. Chem. Int. Ed.*, 2016, **56**, 686.

3 K. Oyaizu and H. Nishide, Conjugated Polymers, 2019, 587. K. Hatakeyama, T. Nagano, S. Noguchi, Y. Sugai, J. Du, H. Nishide and K. Oyaizu, *ACS Appl. Polym. Mater.,* 2019, **1**, 188.

4 R. Emanuelsson, M. Sterby, M. Stromme and M. Sjodin, *J. Am. Chem. Soc.*, 2017, **139**, 4828.

5 F. N. Ajjan, D. Mecerreyes and O. Inganas, *Biotechnol. J.*, 2019, **14**, 1900062.

6 A. M. Navarro-Suárez, J. Carretero-González, N. Casado, D. Mecerreyes, T. Rojo and E. Castillo-Martínez, *Sustain. Energy Fuels*, 2018, **2**, 836.

7 C. Friebe, A. Lex-Balducci and U. S. Schubert, *ChemSusChem*, 2019, **12**, 4093.

8 Y. Y. Lai, X. Li and Y. Zhu, *ACS Appl. Polym. Mater.*, 2020, **2**, 113.

9 N. Casado, G. Hernández, H. Sardón and D. Mecerreyes, *Prog. Polym. Sci.*, 2016, **52**, 107.

10 K. Pirnat, N. Casado, L. Porcarelli, N. Ballard and D. Mecerreyes, *Macromolecules*, 2019, **52**, 8155.

11 L. Zhu, G. Ding, L. Xie, X. Cao, J. Liu, X. Lei and J. Ma, *Chem. Mater.*, 2019, **31**, 8582.

12 H. Wang, R. Emanuelsson, H. Liu, K. Edstrom, F. Mamedov, M. Stromme and M. Sjodin, *ACS Appl. Energy Mater.*, 2019, **2**, 7162.

13 N. Patil, A. Aqil, F. Ouhib, S. Admassie, O. Inganäs, C. Jérôme and C. Detrembleur, *Adv. Mater.*, 2017, **29**, 1703373.

14 T. Liu, K. C. Kim, B. Lee, Z. Chen, S. Noda, S. S. Jang and S. W. Lee, *Energy Environ. Sci.*, 2017, **10**, 205–215.

15 N. Wang, D. Hou, Q. Li, P. Zhang, H. Wei and Y. Mai, *ACS Appl. Energy Mater.*, 2019, **2**, 5816–5823.

16 C. Liedel, X. Wang and M. Antonietti, *Nano Energy*, 2018, **53**, 536–543.

17 I. K. Ilic, M. Perovic and C. Liedel, *ChemSusChem*, 2020, **2020**, cssc.201903156.

18 N. Patil, M. Aqil, A. Aqil, F. Ouhib, R. Marcilla, A. Minoia, R. Lazzaroni, C. Jérôme and C. Detrembleur, *Chem. Mater.*, 2018, **30**, 5831–5835.

19 L. Akerlund, R. Emanuelsson, G. Hernández, F. Ruipérez, N. Casado, D. Brandell, M. Stromme, D. Mecerreyes and M. Sjodin, *ACS Appl. Energy Mater.*, 2019, **2**, 4486.

20 H. N. Nguyen, E. T. Nadres, B. G. Alamani and D. F. Rodrigues, *J. Mater. Chem. B,* 2017, **5**, 6616.

21 J. Xue, Z. Zhang, J. Nie and B. Du, *Macromolecules*, 2017, **50**, 5285.

22 A. D. Becke, *J. Chem. Phys,* 2012, **136**, 150901.

23 J. P. Perdew "Electronic structure of solids '91", Akademie Verlag, Berlin, 1991.

24 K. P. Burke and Y. Wang "Electronic density functional theory: recent progress and new directions", p. 384, Springer, Boston 1998.

25 W. J. Hehre, R. Ditchfield and J. A. Pople, *J. Chem. Phys.*, 1972, **56**, 2257.

26 D. E. Woon and T. H. Dunning, *J. Chem. Phys.*, 1993, **98**, 1358.

27 M. Cossi, V. Barone, R. Cammi and J. Tomasi, *Chem. Phys. Lett.,* 1996, **255**, 327.

28 E. Cancès, B. Mennucci and J. Tomasi, *J. Chem. Phys.*, 1997, **107**, 3032.

Published in : Sustainable Energy & Fuels (2020), pp. 1–10
DOI: 10.1039/D0SE00531B
Status : Postprint (Author's version)

29 V. Barone, M. Cossi and J. Tomasi, *J. Chem. Phys.*, 1997, **107**, 3210.

30 V. Barone, M. Cossi and J. Tomasi, *J. Comput. Chem.*, 1998, **19**, 404.

31 M. J. Frisch, G. W. Trucks, H. B. Schlegel, G. E. Scuseria, M. A. Robb, J. R. Cheeseman, G. Scalmani, V. Barone, G. A. Petersson, H. Nakatsuji, X. Li, M. Caricato, A. V. Marenich, J. Bloino, B. G. Janesko, R. Gomperts, B. Mennucci, H. P. Hratchian, J. V. Ortiz, A. F. Izmaylov, J. L. Sonnenberg, D. Williams-Young, F. Ding, F. Lipparini, F. Egidi, J. Goings, B. Peng, A. Petrone, T. Henderson, D. Ranasinghe, V. G. Zakrzewski, J. Gao, N. Rega, G. Zheng, W. Liang, M. Hada, M. Ehara, K. Toyota, R. Fukuda, J. Hasegawa, M. Ishida, T. Nakajima, Y. Honda, O. Kitao, H. Nakai, T. Vreven, K. Throssell, J. A. Montgomery, Jr., J. E. Peralta, F. Ogliaro, M. J. Bearpark, J. J. Heyd, E. N. Brothers, K. N. Kudin, V. N. Staroverov, T. A. Keith, R. Kobayashi, J. Normand, K. Raghavachari, A. P. Rendell, J. C. Burant, S. S. Iyengar, J. Tomasi, M. Cossi, J. M. Millam, M. Klene, C. Adamo, R. Cammi, J. W. Ochterski, R. L. Martin, K. Morokuma, O. Farkas, J. B. Foresman, and D. J. Fox, *Gaussian, Inc., Wallingford CT*, 2016.

32 N. Patil, C. Jérome and C. Detrembleur, *Prog. Polym. Sci.*, 2018, **82**, 34.

33 S. Skelton, M. Bostwick, K. O'Connor, S. Konst, S. Casey and B. P. Lee, *Soft Matter,* 2013, **9***,* 3825.

34 P. Glass, H. Chung, N. R. Washburn and M. Sitti, *Langmuir,* 2009, **25**, 6607.

35 Y. Xue and H. Xiao, *Polymers,* 2015, ***7,*** 2290.

36 N. V. Salim, N. Hameed, T. L. Hanley and Q. Guo, S*oft. Mater.*, 2013, **9,** 6174.

37 S. W. Kuo, P. H. Tung and F. C. Chang, *Macromolecules*, 2006, **39**, 9388.

38 S. W. Kuo, *J. Polym. Res.*, 2008, **15**, 459.

39 J. Yang, J. Kiejsers, M. van Heek, A. Stuiver, M. A. Cohen Stuart and M. Kamperman, *Polym. Chem.*, 2015, **6**, 3121.

40 A. Kiani, J. RaOof, D. Nematollahi and R. Ojani, *Electroanalysis*, 2005, **17**, 1755.